Materials and Design 188 (2020) 108435

Contents lists available at ScienceDirect

Materials and Design

journal homepage: www.elsevier.com/locate/matdes

An integrated-model for austenite yield strength considering the influence of temperature and strain rate in lean steels

Adriana Eres-Castellanos [a], Isaac Toda-Caraballo [a,*], Andreas Latz [b], Francisca G. Caballero [a], Carlos Garcia-Mateo [a]

[a] National Center for Metallurgical Research (CENIM-CSIC), Av. Gregorio del Amo 8, Madrid 28040, Spain
[b] thyssenkrupp Steel Europe AG, Technology & Innovation, Modelling and Simulation, Kaiser-Wilhelm-Straße 100, 47166 Duisburg, Germany

HIGHLIGHTS

- A large austenite composition-strain rate-temperature-yield strength dataset has been collected.
- The most complete phenomenological models for austenite yield strength are tested.
- An integrated model for the prediction of the austenite yield strength is proposed and tested.
- The proposed model relative error is 96% lower than the relative error of previous models.

GRAPHICAL ABSTRACT

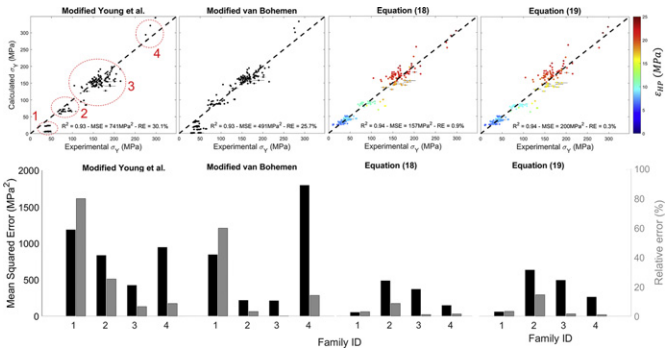

ARTICLE INFO

Article history:
Received 29 October 2019
Received in revised form 11 December 2019
Accepted 16 December 2019
Available online 17 December 2019

Keywords:
Austenite
Yield strength
Hot deformation behavior
Mechanical properties

ABSTRACT

Due to the necessity to exhaustively control the hot deformation of austenite, a strong effort has been made in the past to propose predictive models for the yield strength. Such models have shown accurate predictions within relatively narrow compositional range, closely related to the limitations of the database employed. Nevertheless, by testing those models with a large database, including a wider range of temperatures and compositions, the authors have observed that such narrow compositional ranges cause these models to be inaccurate. The strain rate is also an important parameter that has been ignored in previous works, and deeply affects mechanical behavior. In this work, we propose a more robust model, which includes the contribution of the strain rate and wider composition and temperature ranges by integrating different formulations, providing improvement at predicting yield strength with respect to previous models.

1. Introduction

The increasing requirements of properties for steel parts have made the development of high strength steels an issue of paramount

* Corresponding author.
E-mail address: isaac.toda@cenim.csic.es (I. Toda-Caraballo).

https://doi.org/10.1016/j.matdes.2019.108435

List of abbreviations

A_1, A_2	Constants in Eq. (11)
a	Lattice parameter
α	Constant in Eq. (17)
δ	Ferrite volume percentage
B	Constant in Eq. (10)
B_i	Solid solution coefficient of the element i
b	Constant in Eq. (10)
C, C_3, C_5, C_6	Constants in Eqs. (10) and (11)
C_δ	Strengthening coefficient due to the presence of small amounts of ferrite
C_{HP}	Binary constant that allows to see whether the grain boundary strengthening has been included in the assessed model
CR_1, CR_2	Cooling rates used during single hit compression tests
D	Austenite grain size
ε	Plastic strain
$\dot{\varepsilon}$	Strain rate
$\dot{\varepsilon}_0$	Reference strain rate
ε_{HP}	Confidence interval associated with the grain boundaries strengthening
ε_{loc}	Local atomic misfit
$f(T_{def})$, $f(T_{def}, \varepsilon)$	Temperature and temperature-and-strain-rate dependent functions used in former or proposed models
f_1, f_2	Models 1 and 2 used in the exemplification of the K-Fold Cross-Validation
f_{1-N}, f_{2-N}	Model 1 or 2 trained by using all folds excepting the Nth fold
G	Shear modulus
η_{loc}'	Local shear modulus misfit
HR	Heating rate used during single hit compression tests
JC	Johnson and Cook
K	Number of folds that the database has been divided into for the K-Fold Cross-Validation estimator.
k	Hall-Petch hardening
MSE	Mean Squared Error
MSE_1, MSE_2	Expected prediction error of models f_1 and f_2, obtained by applying the K-Fold Cross-Validation method
$MSE_{1\text{-}N}$, $MSE_{2\text{-}N}$	Mean Squared Error obtained when testing the model f_{1-N} or f_{2-N} with the N fold during the Nth iteration of the K-Fold Cross-Validation method
MZA	Modified Zerilli-Armstrong
m	Constant in Eq. (10)
N	Iteration number during K-Fold Cross-Validation process
n	number of measurements
P	Value of the corresponding parameter shown in Eqs. (15) and (16) obtained by fitting the whole dataset
P_N	Value of the corresponding parameter obtained for the Nth iteration during K-Fold Cross-Validation process
R^2	Correlation
RE	Relative Error
σ_0	Strengthening due to solid solution, work hardening, Peierls friction and precipitation
σ_{PF}	Strengthening due to Peierls friction
σ_{SS}	Solid solution strengthening
σ_Y	Austenite yield strength
σ_{Yref}	Yield strength measured at room temperature (and under quasi-static conditions in case the effect of the strain rate is considered)
SD	Standard Deviation
$\tau(0\ K)$	Critical resolved shear stress for dislocation slip at 0 K
T_γ	Austenitization temperature
t_γ	Austenitization time
T_{def}	Deformation temperature
T_K	Absolute temperature
T_m	Melting temperature
T_r	Temperature increase with respect to room temperature
T_{room}	Room temperature
Y_i	Yield Strength Experimental value i
$\hat{Y}_i$	Yield Strength Predicted value i
W_i	Weight percent of the element i
X_i	Atomic percent of the element i
ZA	Zerilli-Armstrong

importance. Steels are usually subjected to a large variety of thermomechanical treatments to optimize the final properties of the resulting microstructure. These thermomechanical treatments are usually applied when the microstructure is fully austenitic, either above the austenite transformation temperature, Ac3, or at lower temperatures but before austenite decomposition. Nevertheless, as the industrial rolling mills have limitations on the loadings that can be applied into the processed materials, an accurate prediction of the mechanical response of the steel is needed to adjust the processing parameters. The austenite yield strength is a key parameter in this prior analysis [1,2] and, thus, its prediction is indeed useful for the industry. In addition, when only a thermal treatment is employed as a mean to obtain a certain microstructure, e.g. isothermal treatments to obtain bainitic microstructures, the austenite strength also plays an important role in defining the final properties [3,4].

Thus, predicting the austenite yield strength, σ_Y, which depends on composition, strain rate and temperature, is challenging but results in outstanding benefits for the alloy design and performance.

During the last decades, several attempts have been made in order to build predictive models of austenite yield strength at different temperatures, although most of them have focused on austenitic steels because of the simplicity to measure their mechanical properties at low temperatures. For instance, Li et al. [5,6] developed two different models that allowed the estimation of the yield strength of metallic materials, including austenitic stainless steels, at different temperatures, based on the equivalence between heat energy and deformation energy. Those models require the estimation of some variables, such as the Young's modulus or the yield strength at a reference temperature. This makes the model difficult to apply, since further experimental information for each composition considered must be acquired in advance. Sevsek et al. [7] also proposed a model which had the same formulation as previous models [8–10], although it also included a physical term to account for the short-range ordering (SRO) in high-manganese steels. Such a model cannot be generally applied, since SRO is only present in some alloys and its contribution is not easy to quantify. In addition, many other models that do not rely on physical equations have been proposed. Artificial neural networks have been developed [11–13] due to the ability to incorporate non-linear relationships, as required by the mechanical properties behavior at high temperatures. Similarly, phenomenological models in the form of semi-empirical equations have been most commonly used to predict yield strength in austenite [14–17]. Although all of them prove to accurately predict the data they were built with, these models are strongly dependent on the compositional limits defined by their employed database, lacking of generality. In this work a large composition-strain rate-temperature-yield strength database from different sources [4,18–20] has been collected and it has been used to assess the above mentioned phenomenological models. The aim of this study is to develop a more accurate expression for non-pre-strained austenite. Although other works have focused

their attention on the microstructure evolution during recrystallization, including correlation of the stress-strain curves to temperature and strain rate, in many different conditions and steel grades [21–26], we have assumed that previous rolling passes if any, have completely recrystallized the microstructure. Finally, different formulations of models previously published in the literature have been integrated, considering a solid solution strengthening contribution, as well as the effect of both temperature and strain rate.

2. Database

As previously mentioned, the aim of this study is to develop a model that allows to predict the austenite yield strength σ_Y. For that purpose, a database composed of 845 σ_Y measurements on 80 different steels has been collected [4,18–20]. Most of them (98.5% of the measurements) were estimated by the 0.2% criterion from stress-strain curves obtained experimentally from compression tests performed in dilatometers Bahr 805. Fully austenitized samples were cooled down to the corresponding deformation temperature (T_{def}) and were plastically deformed, under different strain rates (ε). Phase transformation and precipitation during the elastic regime or the first stages of the plastic regime were neglected, so it can be assumed that the yield strength value will not be compromised by the presence of second phases.

Table 1 includes all variables that have been taken into account for the present study, all chemical contents have been included in at. %. A set of frequency histograms representing the variation and limits of the variables can be found in Fig. 1, where the bins of the histogram corresponding to the strain rates are logarithmic. As can be seen, all alloying element concentration are below 6 at. % and most of the data lies in between 0 and 2 at. %. Some of the alloys may contain small quantities of elements such as Nb, P or S (below 0.06, 0.07 and 0.03 at. % (0.09, 0.04 and 0.02 wt%), respectively) that have not been included in the study.

Regarding the test temperatures, although most of the data refer to high temperatures (higher than 800 °C), there are also some data in the range 200–700 °C, which means that the model will account for both low and high temperatures. Concerning the strain rates, a large fraction of the data corresponds to strain rates higher than 1 s^{-1}. However, some data taken under quasi-static conditions (0.003 s^{-1}) and under higher strain rates (up to ~11 s^{-1}) have also been considered in order to account for extreme values of this parameter, aimed at increasing the accuracy and the applicability of the model.

The data have been divided into four different families for a better comparison of the results, see Table 2. The families have been selected according to their deformation temperatures and carbon contents and they will be named by their family ID, ranging from 1 to 4. Hence, whereas family 1 corresponds to deformations applied at the highest temperatures (900–1100 °C) and includes values from the lowest carbon steels (0.12–1.65 at. % C (0.03–0.36 wt%)), the range of deformation temperatures of family 2 includes lower temperatures (500–850 °C) and higher carbon contents (1.09–2.21 at. % C (0.24–0.49 wt%)). The temperature ranges of both families 3 and 4 correspond to the lowest temperatures in the database (275–520 °C and 200–350 °C, respectively). However, while family 3 carbon contents lie between 1.36 and 2.21 at. % C (0.30–0.49 wt%), family 4 only contains values from steels with 4.42 at. % C (1 wt%). The results for those families will be compared individually, trying to identify in which ranges the model work better.

3. Experimental

In order to validate the model with data that not been used to build the model, single hit compression tests have been performed in two commercial steels: Sidenor SCM40, Ovako 477L and in a low carbon high silicon modeled steel, named from now on as 02C3Si. These tests are performed in a Bahr 805D high-resolution dilatometer equipped with a deformation module consisting of silicon nitride punchers separated from the sample by molybdenum films in order to reduce friction. The temperature is controlled by type K thermocouple welded to the center of the sample and temperature can be decreased or increased by blowing Helium or by using an induction heating coil, respectively. The changes in length of the sample can be tracked by the dilatometer to study phase transformation occurring during the thermal or thermomechanical treatments. Samples are 10 mm long cylinders, with a radius of 5 mm.

Steels are heated up to the austenitization temperature, T_γ, always higher than the corresponding Ac3 temperature of the steel. T_γ is held for a period of time t_γ and, after that, steels are cooled down to different T_{def}, at which compression is applied at 0.04 s^{-1} up a strain high enough to plastically deform the samples. It must be made sure that no phase transformation occurs during cooling from T_γ to T_{def} by checking that there is no deviation from the linearity during the mentioned step. Before and after the compression takes place, the temperature is held for short periods of time (10–15 s) to make sure that the temperature is homogeneous along the sample (in the case of the first holding) or that the elastic recovery has taken place (in the case of the second holding). The values of the variables used for each single hit compression test depending on the steel can be found in Table 3.

4. Prediction of yield strength

4.1. Previous models in the literature

The yield strength can be approximated by the Hall-Petch relationship [27] as described below:

$$\sigma_Y = \sigma_0 + k \cdot D^{-1/2} \quad (1)$$

where $k \cdot D^{-0.5}$ is the grain boundaries stregthening, k is the Hall-Petch hardening parameter and D is the austenite grain size. The term σ_0 markedly depends on the temperature, composition, strain and strain rate [28]. All the strengthening contributions to the yield strength, with the exception of the grain size strengthening, i.e. solid solution strengthening, work hardening, strengthening due to Peierls friction (stress required to move a dislocation within a plane of atoms in the

Table 1
Input variables minimum (Min) and maximum (Max) values, besides their mean and standard deviation (SD). T_{def} and ε stand for the deformation temperature and strain rate, respectively. The chemical compositions are in at. %, whereas the corresponding equivalence in wt% is in brackets.

	C	Si	Cr	Mo	Mn	Ni	V	Cu	Ti	Al	T_{def} (°C)	ε (s^{-1})
Min.	0.12 (0.03)	0.00 (0.00)	0.01 (0.04)	0.00 (0.00)	0.00 (0.00)	0.00 (0.00)	0.00 (0.00)	0.00 (0.00)	0.00 (0.00)	0.00 (0.00)	200	0.003
Max.	4.42 (1.00)	5.80 (3.05)	1.70 (1.6)	0.37 (0.63)	2.62 (2.60)	1.90 (2.00)	0.22 (0.21)	0.23 (0.26)	0.19 (0.16)	3.63 (1.8)	1100	11
Mean	0.90 (0.20)	1.21 (0.63)	0.45 (0.43)	0.05 (0.09)	1.59 (1.59)	0.10 (0.10)	0.02 (0.02)	0.03 (0.03)	0.04 (0.03)	0.45 (0.22)	890	1.74
SD	0.71 (0.16)	1.16 (0.60)	0.42 (0.41)	0.08 (0.14)	0.47 (0.47)	0.33 (0.35)	0.05 (0.04)	0.04 (0.05)	0.05 (0.05)	0.81 (0.40)	230	2.82

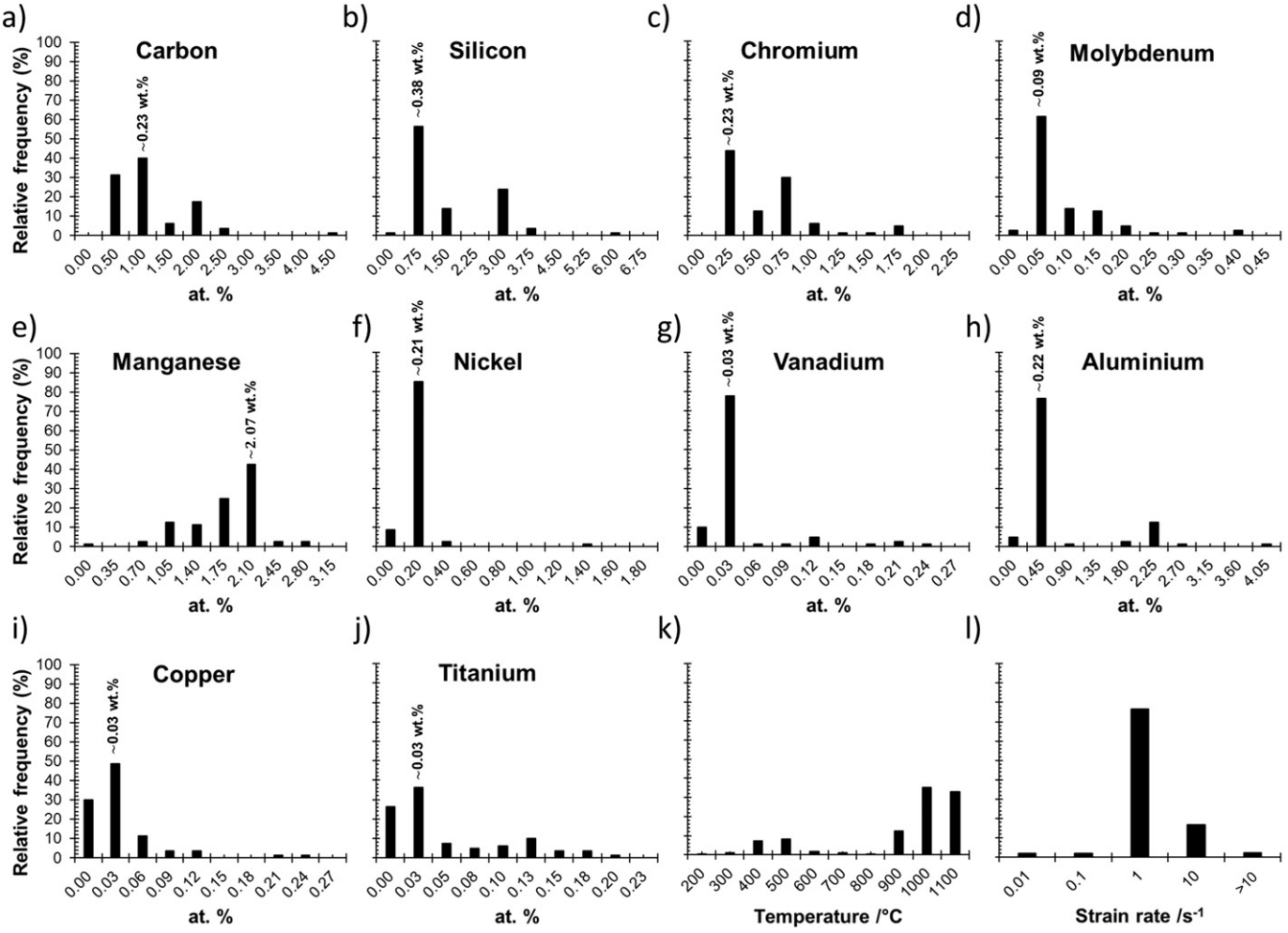

Fig. 1. Histograms of a–j) chemical steel compositions, k) deformation temperatures and l) strain rates corresponding to the σ_Y database used in this work, where the limits, means and standard values of all parameters can be found in Table 1. The approximate equivalence in wt% of the bar with the highest relative frequency can be found on top of the given bar.

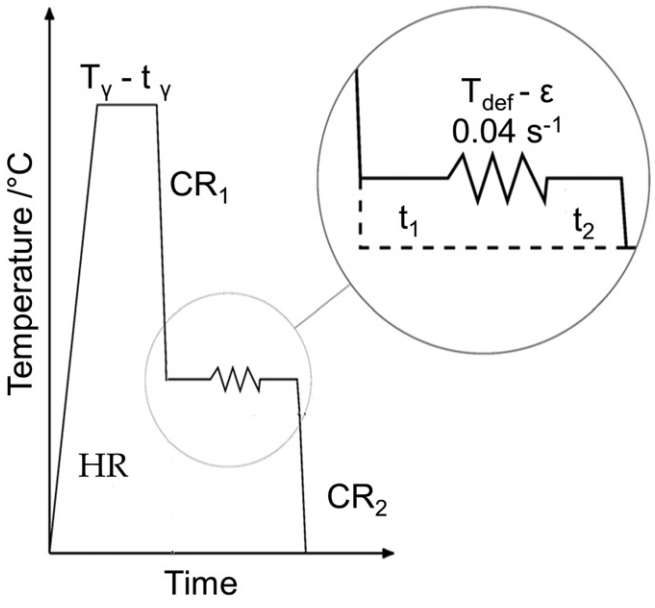

Fig. 2. Sketch of the single hit compression tests performed to further validate the model, where *HR* is the heating rate up to the austenitization temperature, T_γ, and CR_1 and CR_2 are the cooling rates selected for the corresponding steps. t_γ, t_1 and t_2 stand for austenitization time, and time before and after the compression takes place, respectively.

unit cell) or precipitate strengthening, must be contained in σ_0 [29]. However, if samples have not been previously plastically deformed, the work hardening effect is considered negligible. Additionally, under the assumption of no precipitates in the microstructure, the σ_Y expression can be simplified as [14]:

$$\sigma_Y = \sigma_{PF} + \sigma_{SS} + k \cdot D^{-1/2} \tag{2}$$

where σ_{PF} and σ_{SS} are the strengthening due to Peierls friction and solid solution, respectively. For a given temperature, while σ_{PF} is assumed to be a constant, σ_{SS} has been traditionally expressed as the linear combination of the solute content (X_i) and their corresponding coefficients (B_i), i.e. $\sigma_{SS} = \sum_{i=1}^{n} B_i X_i$.

Irvine, using this formulation, derived a regression formula to obtain the yield strength in austenitic stainless steels at room temperature (σ_{Yref}) [14]:

$$\begin{aligned}\sigma_{Yref} = 63.1 + 493W_N + 354W_C + 20.8W_{Si} + 3.70W_{Cr} + 14.5W_{Mo} \\ +18.5W_V + 4.5W_W + 40.0W_{Nb} + 26.2W_{Ti} + 12.6W_{Al} \\ +2.46\delta + k \cdot D^{-1/2}\end{aligned} \tag{3}$$

where W_i denotes the weight percent of the element i and δ is the ferrite volume percentage. The ferrite volume percentage was added by Irvine as the expression was specific for austenitic steels, in which some small fractions of ferrite may be present. It has been proved that the yield strength increases because of the presence of second phases at any given strain, linearly related to the volume fraction of those phases

Table 2
Composition (in at. %), deformation temperature (T_{def}) and strain rate (ε) ranges of the different families that the data have been classified into. The corresponding equivalence in wt% is in brackets.

Family ID	1	2	3	4
C	0.12–1.65 (0.03–0.36)	1.09–2.21 (0.24–0.49)	1.36–2.21 (0.30–0.49)	4.42–4.42 (1.00–1.00)
Si	0–3.01 (0–1.55)	0–3.01 (0–1.58)	1.50–5.80 (0.78–3.05)	2.83–2.83 (1.50–1.50)
Cr	0.01–1.70 (0.01–1.60)	0.16–1.55 (0.15–1.49)	0.49–1.56 (0.47–1.50)	1.33–1.33 (1.30–1.30)
Mo	0–0.37 (0–0.63)	0–0.18 (0–0.31)	0–0.23 (0–0.40)	0–0 (0–0)
Mn	0–2.62 (0–2.60)	0–1.98 (0–2.01)	0.69–1.98 (0.71–2.01)	1.83–1.83 (1.9–1.9)
Ni	0–1.90 (0–2.00)	0–1.36 (0.01–1.45)	0–1.84 (0–2.00)	0–0 (0–0)
V	0–0.22 (0–0.21)	0–0.11 (0–0.10)	0–0.11 (0–0.10)	0–0 (0–0)
Cu	0–0.23 (0–0.26)	0–0.01 (0–0.02)	0–0.12 (0–0.14)	0–0 (0–0)
Ti	0–0.19 (0–0.16)	0–0.04 (0–0.03)	0–0.01 (0–0.01)	0–0 (0–0)
Al	0.02–3.63 (0–1.80)	0–2.13 (0–1.07)	0–2.13 (0–1.07)	0–0 (0–0)
T_{def} (°C)	900–1100	500–850	275–520	200–350
ε (s^{-1})	0.01–11	0.02–0.88	0.003–0.5	0.003–0.003
σ_Y (MPa)	7–66	68–135	105–215	275–298
Number of measurements	600	100	141	4

[14]. Note that these volume fractions are always low and the main phase is in all cases austenite. Moreover, although the austenite yield strength depends on composition, the effect of the ferrite into the total yield strength is non-compositional dependent, lacking the effect of alloying elements in the ferrite. For the sake of clarity, all stress units in this work will be MPa.

Irvine's relation has been tested in the literature for some chemical compositions and conditions, e.g. it was concluded that the model could not successfully predict the yield strength for some austenitic TWIP steels [15,30], whose chemical composition is different to the ones contained in Irvine's database. Van Bohemen attributed the difference to the fact that Irvine had used data from steels which were rather low in C (0.28–0.46 at. % (0.06–0.1 wt%)), whereas they were high in Ni and Cr [15]. For that reason, while the contributions of C, Si, Cr and Al seem to have been overestimated, the significance of the Peierls friction strengthening seems to be much higher than expected by Irvine [15,30,31]. Thus, van Bohemen proposed a new expression (Eq. (4)), which is consistent with his results of austenitic TWIP steels. Note that he omitted N and δ as it was not included in their database [15].

$$\sigma_{Yref} = 87.8 + 354W_C + 15.1W_{Si} + 2.5W_{Cr} + 14.5W_{Mo} + 18.5W_V + 4.5W_W + 40.0W_{Nb} + 26.2W_{Ti} + 5.4W_{Al} + k \cdot D^{-1/2} \quad (4)$$

Young et al. [17] developed an expression (Eq. (5)) that also takes into account the temperature effect on the austenite yield strength, assuming no ferrite present. This expression is composed of the product of two terms. The former one is a summation in the form of Irvine's [14], which shares most of its coefficients, although $k \cdot D^{-1/2}$, W_{Nb}, W_V, W_{Ti}, W_W and W_{Al} have been omitted. The second term, $f(T_{def})$, accounts for the variability of σ_Y with temperature:

$$\sigma_Y = (67.8 + 493W_N + 354W_C + 20.8W_{Si} + 3.70W_{Cr} + 14.5W_{Mo}) \times \left(1 - 0.26 \cdot 10^{-2}T_r + 0.47 \cdot 10^{-5}T_r^2 - 0.326 \cdot 10^{-8}T_r^3\right) \quad (5)$$

where T_r is the temperature increase with respect to room temperature, T_{room}, ($T_r = T_{def} - T_{room}$, T_{def} is the deformation temperature). Such expression has been widely used by some other authors, especially when assessing the yield strength for the design of bainitic microstructures [32–35].

Azuma et al. [16] modified Young et al.'s equation to include the effect of manganese on the yield strength, according to Irvine [14], which reads as follows:

$$\sigma_Y = (55.4 + 493W_N + 354W_C + 20.8W_{Si} + 3.70W_{Cr} + 14.5W_{Mo} + 10.0W_{Mn}) \times \left(1 - 0.26 \cdot 10^{-2}T_r + 0.47 \cdot 10^{-5}T_r^2 - 0.326 \cdot 10^{-8}T_r^3\right) \quad (6)$$

However, Bhadeshia later pointed out that Azuma's equation had been stated incorrectly [36].

In addition to the previously described modification of Irvine's expression, van Bohemen also proposed a new formulation for the temperature dependency, also using a polynomial function, $f(T_{def})$ [15]:

$$\sigma_Y = (87.8 + 354W_C + 15.1W_{Si} + 2.5W_{Cr} + 14.5W_{Mo} + 18.5W_V + 4.5W_W + 40.0W_{Nb} + 26.2W_{Ti} + 5.4W_{Al} + k \cdot D^{-0.5}) \left(1 - 0.22 \cdot 10^{-2}T_r + 0.42 \cdot 10^{-5}T_r^2 - 0.3 \cdot 10^{-8}T_r^3\right) \quad (7)$$

Table 3
Values of the single hit compression tests parameters found in Fig. 2.

Steel	*HR* (°C/s)	T_γ (°C)	t_γ (s)	CR_1 (°C/s)	T_{def} (°C)	CR_2 (°C/s)
Sidenor SCM40	5	990	240	15	520 400 300	25
02C2Si	5	900	240	30	530 410	25
Ovako 477L	5	965	240	20	510 390 340	25

In order to simplify comparison between the proposed models, the different coefficients used by all these authors can be found in Table 4. The formulas have the form of: $\sigma_Y = (\sigma_{PF} + \sum_{i=1}^{n} B_iW_i + C_\delta\delta + C_{HP} \cdot k \cdot D^{-0.5}) \cdot f(T_r)$, where C_δ is the strengthening coefficient due to the presence of small amounts of ferrite ($MPa{\cdot}\%^{-1}$), which only Irvine incorporated to his expression, and C_{HP} is a binary constant that allows to see whether the grain boundary strengthening has been included. The rest of the parameters have been previously described in the main text.

Table 4
Coefficients of different expressions proposed for yield strength σ_Y as a function of the deformation temperature.

Model	Irvine [7] Eq. (3)	Van Bohemen [8] Eq. (4)	Young et al. [10] Eq. (5)	Azuma et al. [9] Eq. (6)	van Bohemen [8] Eq. (7)
σ_{PF}	63.1	87.8	67.8	55.4	87.8
B_C	354	354	354	354	354
B_N	493	0	493	493	
B_{Si}	20.8	15.1	20.8	20.8	15.1
B_{Cr}	3.7	2.5	3.7	3.7	2.5
B_{Mo}	14.5	14.5	14.5	14.5	14.5
B_{Mn}				10	
B_V	18.5	18.5			18.5
B_W	4.5	4.5			4.5
B_{Nb}	40	40			40
B_{Ti}	26.2	26.2			26.2
B_{Al}	12.6	5.4			5.4
C_δ	2.46				
C_{HP}		1			1
$f(T_r)$	1	1	1 $-0.26\cdot10^{-2}\cdot T_r$ $+0.47\cdot10^{-5}\cdot T_r^2$ $-0.326\cdot10^{-8}\cdot T_r^3$	1 $-0.26\cdot10^{-2}\cdot T_r$ $+0.47\cdot10^{-5}\cdot T_r^2$ $-0.326\cdot10^{-8}\cdot T_r^3$	1 $-0.22\cdot10^{-2}\cdot T_r$ $+0.42\cdot10^{-5}\cdot T_r^2$ $-0.3\cdot10^{-8}\cdot T_r^3$

Because the Young et al.'s model (Eq. (5)) has been extensively used, and because the van Bohemen's model (Eq. (7)) is one of the most complete up to date and also includes most of the elements that can be found in the database considered for this work, both models have been used to test their performance. The model by Irvine is excluded from this comparison since it does not asses the effect of temperature on yield strength.

The evolution of $f(T_{def})$ with temperature for both models can be seen in Fig. 3a, where it is clear that both curves have similar trends, although they are shifted vertically with respect to the other. It is important to remark that both Young et al. and van Bohemen models are only valid for temperatures lower than approximately 960 and 1000 °C, respectively, as the function that governs the effect of temperature becomes negative for higher temperature values.

Results of these models and the subsequently proposed ones that will be tested in this work will be presented in two different ways: a) results for the whole database, in terms of correlation (R^2), Mean Squared Error ($MSE=\frac{1}{n}\sum_{i=1}^{i=n}(Y_i-\hat{Y}_i)^2$, where n is the number of measurements and Y_i and $\hat{Y}_i$ are the experimental and predicted values, respectively) and Relative Error ($RE=\frac{1}{n}\sum_{i=1}^{i=n}|Y_i-\hat{Y}_i|/Y_i$) and b) results for the families described in Table 2 in terms of R^2, MSE and RE.

Neither Young et al.'s nor van Bohemen's models could be evaluated with the data from our database as both models consider neither Mn nor Ni and there are no steels lacking of both elements at the same time in the database. Therefore, the contribution of the elements that were not considered by those models has been fitted in this work, minimizing the RE by using the optimization toolbox implemented in MatLab®, which used the Nelder-Mead method [37], suitable for multidimensional space minimizations. The Nelder-Mead method uses the simplex search method to find iteratively minimum values until the error tolerance is reached. Only yield strengths obtained at temperatures higher than 960 and 1000 °C have been used for the optimization of the parameters describing the modified Young et al.'s and van Bohemen's models, respectively, as the function that describes the evolution of yield strength with temperature in the original models becomes negative for higher temperatures. Eqs. (8) and (9) are the modified Young et al.'s and van Bohemen's,

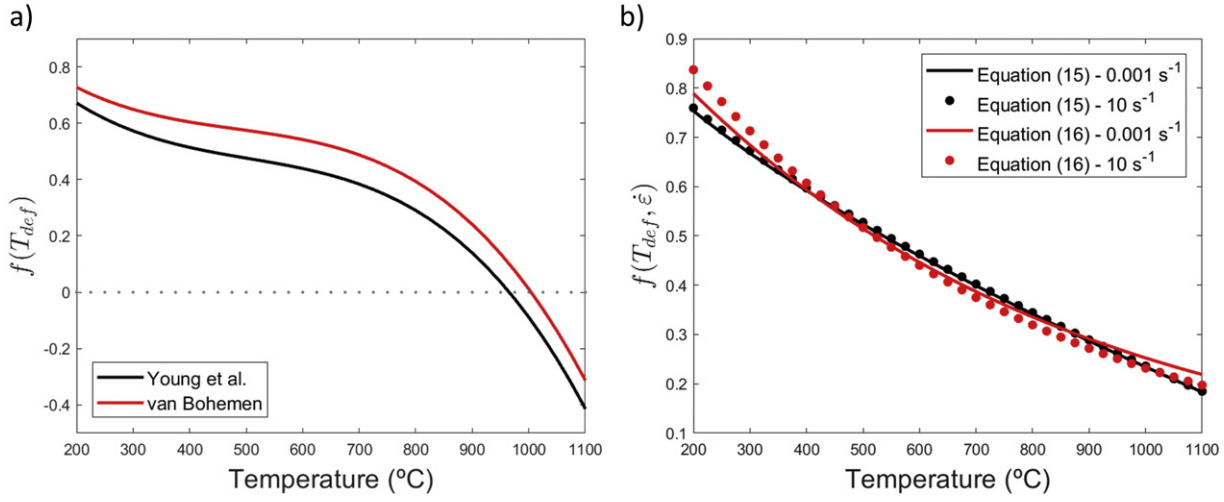

Fig. 3. a) Evolution of the temperature-dependent function, $f(T_{def})$, used by the models developed by Young et al. and van Bohemen; b) evolution of the temperature and strain rate dependent functions, $f(T_{def},\dot{\varepsilon})$, implemented in the model expressed in Eqs. (15) and (16).

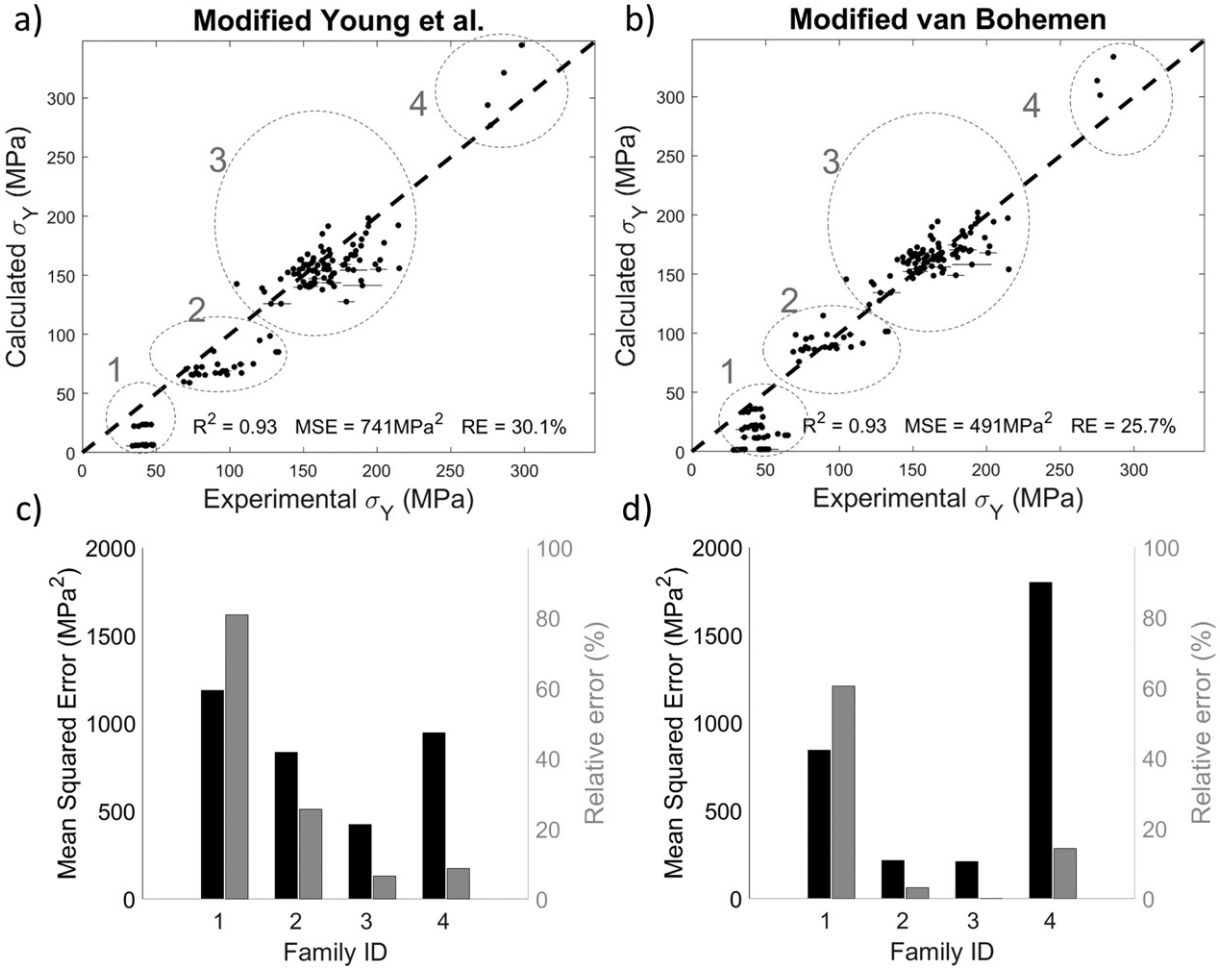

Fig. 4. a–b) Calculated vs. experimental yield strength calculated according to modified Young et al.'s model (Eq. (8)); and modified van Bohemen's model (Eq. (9)). The data corresponds to the whole database and the horizontal lines represent their Experimental Standard Errors. To make the plot clearer, the whole dataset has not been plotted. Instead, the data of steels whose composition is extremely close (close enough not to obtain significant variations of yield strength according to the model) have been averaged, with the horizontal lines representing the confidence interval (Standard Error of the experimental data). The obtained correlation R^2, MSE and RE are on the bottom part of the figure. The data belonging to each of the families described in Table 2 are circled by a grey dashed line, and the family ID is by each circle. c–d) MSE and RE obtained by the modified Young et al.'s and the modified van Bohemen's models. Errors have been calculated family by family, where the family ID is in accordance with Table 2.

respectively.

$$\sigma_Y = (67.8 + 493W_N + 354W_C + 20.8W_{Si} + 3.70W_{Cr} + 14.5W_{Mo} + \mathbf{1.9W_{Mn}} + \mathbf{0.2W_{Ni}} + \mathbf{0.1W_V} + \mathbf{0.4W_{Al}} + \mathbf{0.4W_{Cu}} + \mathbf{0.2W_{Ti}}) \times \left(\mathbf{1 - 0.26 \cdot 10^{-2}} T_r + \mathbf{0.47 \cdot 10^{-5}} T_r^2 - \mathbf{0.326 \cdot 10^{-8}} T_r^3\right) \quad (8)$$

$$\sigma_Y = (87.8 + 354W_C + 15.1W_{Si} + 2.5W_{Cr} + 14.5W_{Mo} + 18.5W_V + 4.5W_W + 40.0W_{Nb} + 26.2W_{Ti} + 5.4W_{Al} + \mathbf{8.1W_{Mn}} + \mathbf{0.2W_{Ni}} + \mathbf{12.8W_{Cu}}) \times \left(\mathbf{1 - 2.2 \cdot 10^{-3}} T_r + \mathbf{4.2 \cdot 10^{-6}} T_r^2 - \mathbf{3.0 \cdot 10^{-9}} T_r^3\right) \quad (9)$$

These modifications have been tested with our database, finding a good but insufficient agreement, as seen in Fig. 4a and b, since the relative errors are always higher than 25%. Also, it is important to remark, as already mentioned, that there have been some data (high temperature) that have been removed from the database as the predictions at such temperatures are always negative. To make the plot clearer, the whole dataset has not been plotted. Instead, the data of steels whose composition is extremely close (close enough not to obtain significant variations of yield strength according to the model) have been averaged, with the horizontal lines representing the confidence interval (Experimental Standard Error).

Fig. 4c and d shows the MSE and RE of the modified Young and Bohemen models by families, and it can be concluded that, while for families 2 and 3 (intermediate and low T_{def}, respectively) the best predictions are given by the modified van Bohemen's equation, the modified Young's equation only seems to be accurate for family 3 (low T_{def} and carbon content between 1.36 and 2.21 at. %). Both modified models fail for the rest of the families.

Although the effect of temperature on the yield strength has been assessed by the previous authors by simple polynomic approaches, there have been many models describing the flow behavior in metallic materials. Two of the most used models to predict flow behavior were proposed by Johnson and Cook (JC) [38,39] and Zerilli-Armstrong (ZA) [40], which can be found in Eqs. (10) and (11), respectively.

$$\sigma = \left(\sigma_{Yref} + B \cdot \varepsilon^b\right) \cdot \left(1 + C \cdot \ln\left(\frac{\varepsilon}{\varepsilon_0}\right)\right) \cdot \left(1 - \left(\frac{T_r}{T_m - T_{room}}\right)^m\right) \quad (10)$$

$$\sigma = \left(\sigma_{Yref} + B \cdot \varepsilon^b\right) \cdot \exp(-A_1 \cdot T_K + A_2 \cdot T_r \cdot \ln(\varepsilon)) \quad (11)$$

where ε is the plastic strain, ε_0 is the reference strain rate, T_m is the steel melting temperature and B, b, C, m, A_1 and A_2 are constants. The JC model is purely phenomenological and it requires a low amount of material constants, which dramatically simplifies the analysis. The JC model has

successfully been applied for various materials, including steel [41], for different ranges of temperature and strain rates [42–44], although it was initially proposed as a model to predict the flow stress behavior for metals subjected to large strains, high strain rates and high temperatures. However, in some other cases, it has been proven not to be accurate [41,45–48] or only be valid in a narrow domain near the reference strain rate, which is fixed in the parameters fitting [46].

Samantaray et al. [45] claimed that the JC model is inadequate to describe their steels' flow behavior as it does not incorporate the coupled effects of strain-temperature and strain rate-temperature, i.e. there are no terms where the effects of the strain or of the strain rate depend on the effect of the temperature, or vice versa [49]. In order to consider those effects, several modifications have been proposed [50–54], although such models have been usually tested with small datasets with limited compositional ranges and will not be described in this work.

On the other hand, the ZA model, widely used for bcc and fcc materials, does take into account coupled effects of strain-temperature and strain rate-temperature on the flow behavior. However, it is expected to apply for very high strain rates and relatively low temperatures (lower than half the correspondent melting temperature) [40].

Based on ZA, several modified models have been proposed [45,55–57]. For fcc materials, the original model and most of its modifications assume that the yield strength (σ_Y) varies with neither temperature nor strain rate, as the only part of the equation that does not depend on the strain is a constant. However, several studies have proven the dependence of σ_Y on both the temperature and the strain rate [58–60]. There are some modifications of the ZA model that include the effect of both the temperature and the strain rate on the σ_Y [45,57], among them the model proposed by Samantaray et al. (Modified ZA, MZA) [45]:

$$\sigma = \left(\sigma_{Yref} + B \cdot \varepsilon^b\right) \cdot \exp\left(-(C_3 + C_4\varepsilon)\cdot T_r + (C_5 + C_6 \cdot T_r)\cdot \ln\left(\frac{\varepsilon}{\varepsilon_0}\right)\right) \quad (12)$$

where C_3, C_4, C_5 and C_6 are constants whose notation has been inherited from the original sources. This model also considers the previously mentioned coupled effects in both the yield strength and the whole flow behavior, which makes its accuracy higher compared to the JC and ZA models [41,45–48]. Additionally, the MZA model is suitable for all ranges of strain rates and temperatures [45,46,48,61–64] provided that the influence of dynamic recovery and dynamic recrystallization is low or negligible [46], although it does not correctly depict flow behavior at high strain levels [65].

4.2. Building the model

In the present study, a similar formulation to Irvine's [14] has been taken. No work hardening term has been included as all steels had not been previously strained, neither the precipitation term has been considered as it depends on many (not reported) parameters, i.e. presence of primary precipitates, austenitization temperature and cooling rate to deformation temperature, and therefore the prediction of what type of precipitates are in the microstructure (if present) and in which amount would be speculative and misleading.

For the purpose of calculating σ_Y for a given T_{def}, ε and chemical composition, the reference yield strength must be multiplied by a function of T_{def} and ε, $f(T_{def}, \varepsilon)$, in the following way:

$$\sigma_Y = \sigma_{Yref} \cdot f(T_{def}, \varepsilon) \quad (13)$$

where σ_{Yref} represents the yield strength at T_{room} and under ε_0. Note that, as concluded by Schwer [66], the constitutive model parameters should be calibrated to the quasi-static strain rate in order to obtain good results. For that reason, ε_0 has been taken as 0.001 s^{-1} in this study. For the sake of clarity, note that the functions $f(T_{def})$ of Eqs. (5), (6) and (7) and $f(T_{def}, \varepsilon)$ of Eq. (13) have different expressions but have the same notation since they represent the dependence of yield strength not related to composition.

Given that the information about prior austenite grain size is limited and incomplete, not allowing to perform a full analysis of the effect of such parameter, in the present model it will be assumed that the grain size strengthening could take values correspondent to typical austenite grain sizes (D) (10–200 μm) [67–69]. Therefore, the grain strengthening term in σ_{Yref} will be formed by the mean of such strengthening values and its confidence interval, which equals the correspondent absolute errors of the strengthening obtained for both limits. Such strengthening values have been calculated according to the Hall-Petch relationship previously mentioned in Eq. (1), where k has been taken as 274 MPa $\mu m^{1/2}$, as reported by Rajasekhara et al. [70] and in good agreement with the value reported by Matsuoka et al. [67]. Thus, the grain size strengthening at room temperature and at the reference strain rate will be assumed to be 53 (±34) MPa:

$$\sigma_Y = \sigma_{Yref} \cdot f(T_{def}, \varepsilon) = (\sigma_{PF} + \sigma_{SS} + 53(\pm 34)) \cdot f(T_{def}, \varepsilon) \quad (14)$$

Bear in mind that the confidence interval associated with the grain boundaries strengthening, ε_{HP}, also depends on temperature and strain rate and it has been assumed that this dependence is similar to the dependence of $\sigma_{PF} + \sigma_{SS}$.

The term σ_{SS} is equal to the summation of the product of the n solute contents in at.% (X_i) and their corresponding solid solution coefficients (B_i):

$$\sigma_Y = \left(\sigma_{PF} + \sum_{i=1}^{n} B_i X_i + 53(\pm 34)\right) \cdot f(T_{def}, \varepsilon) \quad (15)$$

Note that the solute contents are expressed in at. % as the solid solution strengthening depends on the number of atoms that are present in a cell structure rather than their weight.

To consider the effect of temperature and strain rate, $f(T_{def}, \varepsilon)$, based on the literature review shown in the previous subchapter, we have considered taking a similar formulation to the one of the JC and MZA models, with the intention of testing their capabilities at extending their use in wider compositional, temperature and strain rate ranges. Consequently, considering JC and MZA expressions, $\sigma_Y = \sigma_{Yref} \cdot f(T_{def}, \varepsilon)$ can be rewritten as:

$$\sigma_{Y-1} = \sigma_{Yref} \cdot \left(1 + C \cdot \ln\left(\frac{\varepsilon}{\varepsilon_0}\right)\right) \cdot \left(1 - \left(\frac{T_r}{T_m - T_{room}}\right)^m\right) \quad (16)$$

$$\sigma_{Y-2} = \sigma_{Yref} \cdot \exp\left(-C_3 \cdot T_r + (C_5 + C_6 \cdot T_r)\cdot \ln\left(\frac{\varepsilon}{\varepsilon_0}\right)\right) \quad (17)$$

where T_m has been taken as 1473 °C and where the term $B \cdot \varepsilon^b$ in Eqs. (10) and (11) has been removed since no plastic regime is analyzed here. It is noteworthy to say that both expressions share the same σ_{Yref} as the yield strength at the reference state must be identical regardless the chosen expression.

The model parameters have been fitted by using the Nelder-Mead method until the relative error was minimal. The two obtained σ_Y expressions that have been proposed for the current work are:

$$\sigma_{Y-1} = (52.3 + 47.0X_C + 31.3X_{Si} + 1.0X_{Mn} + 1.0X_{Cr} + 31.3X_{Mo} + 1.3X_{Ni} + 10.7X_V + 3.8X_{Al} + 16.8X_{Cu} + 15.2X_{Ti} + 53(\pm 34))\left(1 + 0.001 \ln\left(\frac{\varepsilon}{0.001}\right)\right) \times \left(1 - \left(\frac{T_r}{1487 - 25}\right)^{0.658}\right) \quad (18)$$

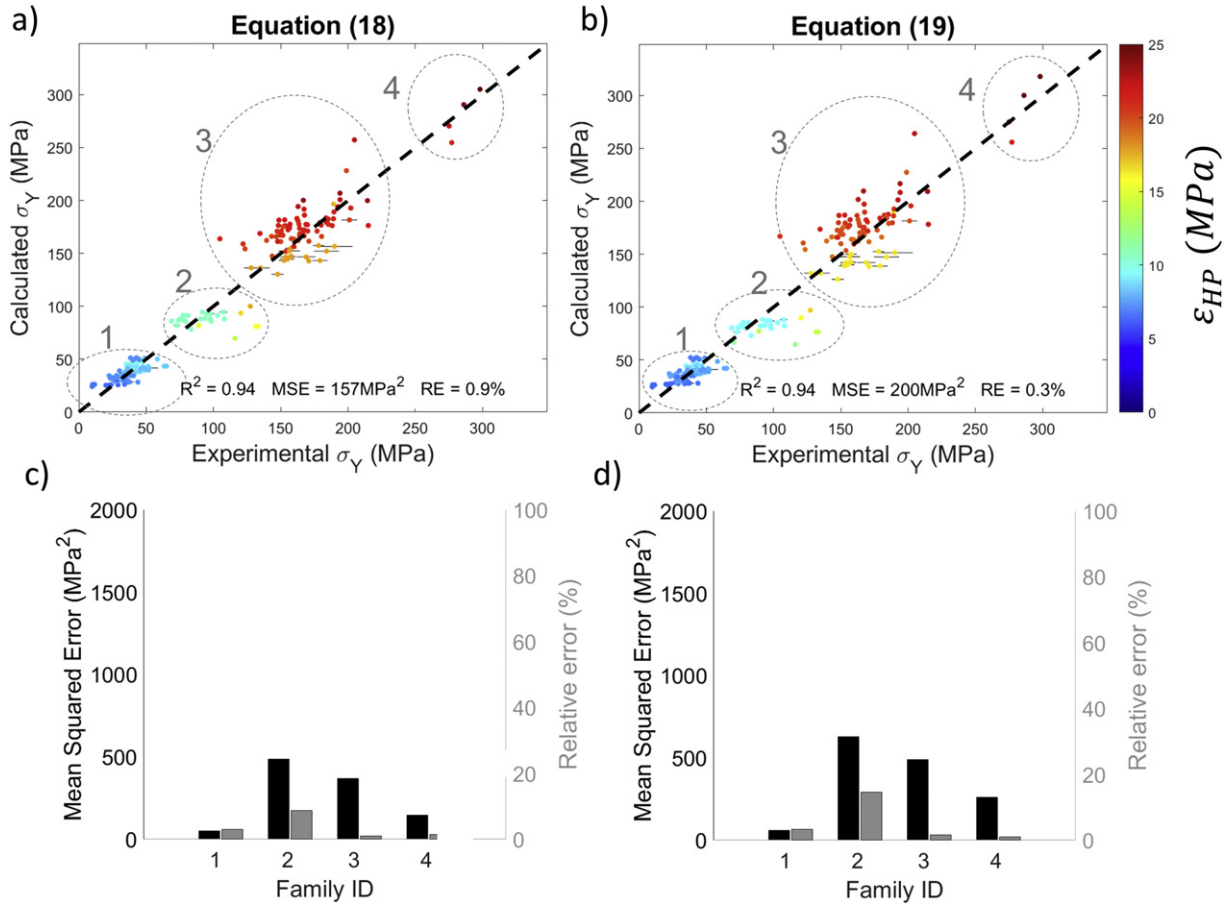

Fig. 5. a–b) Experimental vs. calculated σ_Y calculated according to Eqs. (18) and (19). To make the plot clearer, the whole dataset has not been plotted. Instead, the data of steels whose composition is extremely close (close enough not to obtain significant variations of yield strength according to the model) has been averaged, with the horizontal lines representing the confidence interval (Experimental Standard Error). The color of each point represents ε_{HP}. The obtained correlation R^2, MSE and RE are on the bottom part of the figure. The data belonging to each of the families described in Table 2 are circled by a grey dashed line, and the family ID is by each circle. c–d) MSE and RE obtained by proposed model in Eqs. (18) and (19). The data correspond to the whole database. Errors have been calculated family by family, where the family ID is in accordance with Table 2.

$$\sigma_{Y-2} = \left(52.6 + 50.7X_C + 34.1X_{Si} + 0.9X_{Mn} + 0.6X_{Cr} + 34.1X_{Mo} + 2.3X_{Ni} + 12.3X_V + 6.5X_{Al} + 19.1X_{Cu} + 17.4X_{Ti} + 53(\pm 34)\right) \cdot \exp\left(-0.0014 \cdot T_r + \left(0.0111 - 2.2 \cdot 10^{-5} \cdot T_r\right) \cdot \ln\left(\frac{\varepsilon}{0.001}\right)\right) \quad (19)$$

The temperature and strain rate dependency of the model can be found in Fig. 3b. As can be observed, the model mainly depends on temperature, although some variations with strain rate can be found mainly for Eq. (19). It is important to mention that, for Eq. (19), the effect of the strain rate is reversed for temperatures higher than ~500 °C. Whereas yield strengths increase with strain rate for the lower temperatures, they decrease with strain rate for the highest temperatures. Similar effects have been observed in austenitic stainless steels for similar temperatures in previous works [71–73].

4.3. Validation of the model

The σ_Y calculated by using Eqs. (18) and (19) is in good agreement with the experimental data, as can be observed in Fig. 5a and b. As in the previous occasion, and for the sake of clarity, in the same figure, the whole dataset has not been plotted. Instead, the data of steels whose composition is extremely close (close enough not to obtain significant variations of yield strength according to the model) has been averaged, with the horizontal lines representing the confidence interval (Standard Error of the experimental data). High correlations, i.e. $R^2 = 0.94$, have been obtained in both cases. Although these correlations are only slightly higher than the ones obtained for the modified versions of Young et al. and van Bohemen (Eqs. (8) and (9)), there are two reason why it can be assumed that a much better fitting has been achieved by the proposed model: a) while the MSE are approximately half the ones obtained by applying Eqs. (8) and (9); the RE is one order of magnitude lower than the ones obtained by applying such equations; and b) Eqs. (8) and (9) do not apply for T_{def} higher than 960 and 1000 °C, respectively, whereas Eqs. (18) and (19) are valid for any T_{def} up to 1100 °C.

When analyzing by families, see Fig. 5c and d, although the RE are slightly higher for families 2 and 3 than they were for the modified van Bohemen's model, it can be observed that the errors of both Eqs. (18) and (19) are more constant regardless the family that is analyzed, which indicates that the model does not depend on the compositional range as much as the modified versions of the former models.

5. Results and discussion

5.1. Model predictive capability

As has been previously discussed, the validity of previous models has been proved to be limited, because they were fitted with small datasets and they can then not be generalized to independent datasets. For that reason, in order to compare the capability of Eqs. (16) and (17) to generalize to unseen data, the uncertainty of the estimations given by both equations has been calculated

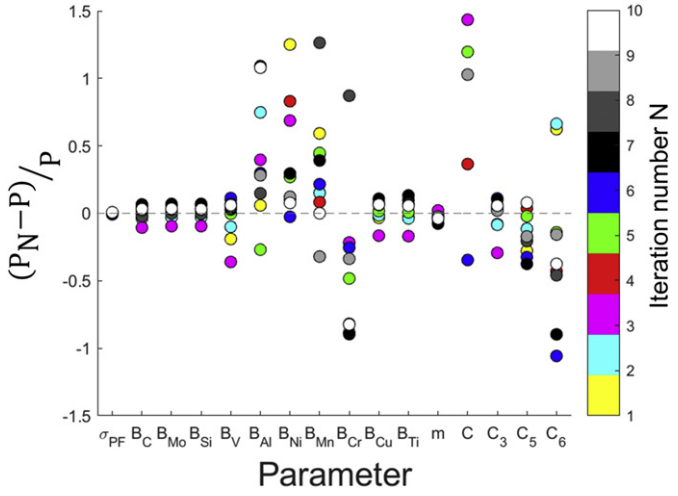

Fig. 6. Relative change in each of the parameter fitted during the K-Fold Cross-Validation method. P_N is the value of the corresponding parameter obtained for the Nth iteration, where the iteration number is defined by the dot color. P is the value of the corresponding parameter shown in Eqs. (18) and (19) and obtained by fitting the whole dataset.

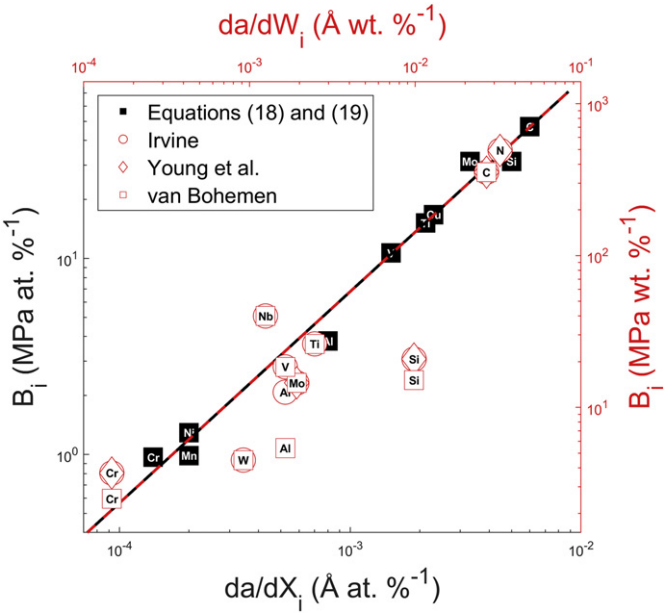

Fig. 7. Solid solution strengthening coefficients of the proposed model (B_i) and the former mentioned models vs. lattice parameter change per atomic percentage ($\frac{da}{dX_i}$) or per weight percentage ($\frac{da}{dW_i}$), extracted from Pearson [81] and Irvine [14]. The white and red symbols correspond to the red axes, whereas the black squares correspond to the black axes. The red and black lines are the lines describing the linear regression of the corresponding data.

according to the K-Fold Cross-Validation estimator [74], see Appendix A for further explanation of the method. In this work, K has been set as ten, as recommended by Kohavi [75].

Fig. 6 shows the relative change $(P_N - P)/P$, where P_N is the value of the corresponding parameter obtained for the Nth iteration and P is the value of the corresponding parameter shown in Eqs. (18) and (19) and obtained by fitting the whole dataset for each of the parameters fitted during the K iterations. It can be seen that some of the parameters double their value for some iterations with respect to the values obtained by fitting the whole database, whereas some of them always keep approximately the same value. It is noteworthy to say that the parameters for which the most pronounced variability has been detected are the ones which have low P values, such as C or B_{Ni}, whereas parameters such as B_C, which are several orders of magnitude higher keep a low relative change. Therefore, it is possible that, even though the relative change of those parameters is rather high, the impact in the final contribution to yield strength is not significant.

The obtained expected prediction errors obtained for both Eqs. (16) and (17) are 162 ± 11 and 207 ± 13 MPa^2, respectively, which indicates that there is a high chance of obtaining accurate predictions when predicting yield strengths for steels, temperatures or strain rates that are not present in the database in both cases, as both errors are low. In addition, as the expected prediction error is lower for Eq. (16) than for Eq. (17), it can be said that the JC model depicts the effect of temperature and strain rate in a more accurate way than the MZA model, even though the literature suggests that MZA is more accurate for any kind of strain rate or temperature.

5.2. Model physical meaning

The reference Peierls friction coefficient ($\sigma_{PF} = 52.6$ MPa) is in agreement with previous values of the literature, as it is of the same order of magnitude than the values obtained by Irvine (63.1 MPa) [14], Young et al. (67.8 MPa) [17] and van Bohemen (87.8 MPa) [15] and it is also comparable to the one evaluated by Kang et al. (87 MPa) [76].

Regarding the solid solution coefficients B_i, it is possible to study whether they have physical meaning by studying the distortion that their corresponding element atoms introduce in the lattice. According to the solid solution strengthening model proposed by Labush [77], the solid solution strengthening effect in FCC alloys can be expressed as:

$$\frac{\tau(0\,K)}{G} \propto \left(\eta'^{2}_{loc} + \alpha^2 \varepsilon^2_{loc}\right)^{\frac{2}{3}} \tag{20}$$

where $\tau(0\,K)$ is the critical resolved shear stress for dislocation slip at 0 K, G is the shear modulus, η_{loc}' is the local shear modulus misfit, ε_{loc} is the local atomic size misfit, i.e. local lattice distortion, and α is a constant. However, $\alpha^2\varepsilon^2_{loc}$ has been found to be much higher than $\eta_{loc}'^2$, which means that the main parameter to study solid solution hardening effect is ε_{loc}, which is proportional to the change in the lattice parameter a with respect to composition, $da/(dX_i)$ [78,79]. Therefore, the solid solution strengthening contribution of all elements must be proportional to their atomic size misfit and, in turn, to $da/(dX_i)$:

$$\frac{\tau(0\,K)}{G} \propto \varepsilon_{loc} \propto \frac{da}{dX_i} \tag{21}$$

This approach has been successful for predicting this effect in compositionally complex alloys [78–80].

The B_i parameters of Eqs. (6), (7), (15) and (16) have been compared to the experimental data on the variation of cell parameter with solute content [14,81]. Since such variation is usually reported in Å at. %$^{-1}$, in order to compare the B_i of the models of Irvine, Young et al. and van Bohemen, $da/(dX_i)$ has been converted to $da/(dW_i)$, assuming that the system that those data have been obtained from is binary. Due to the nature of the solutes, we can assume that most of their interactions are only with Fe, and no crossed interactions between solute atoms are considered or relevant, then, the input from binary systems is suitable for this calculation. The results are shown in Fig. 7, where a good correlation is found in all cases regardless the equation, although the correlation is higher for the model proposed in this work, suggesting that the proposed model is more physically consistent.

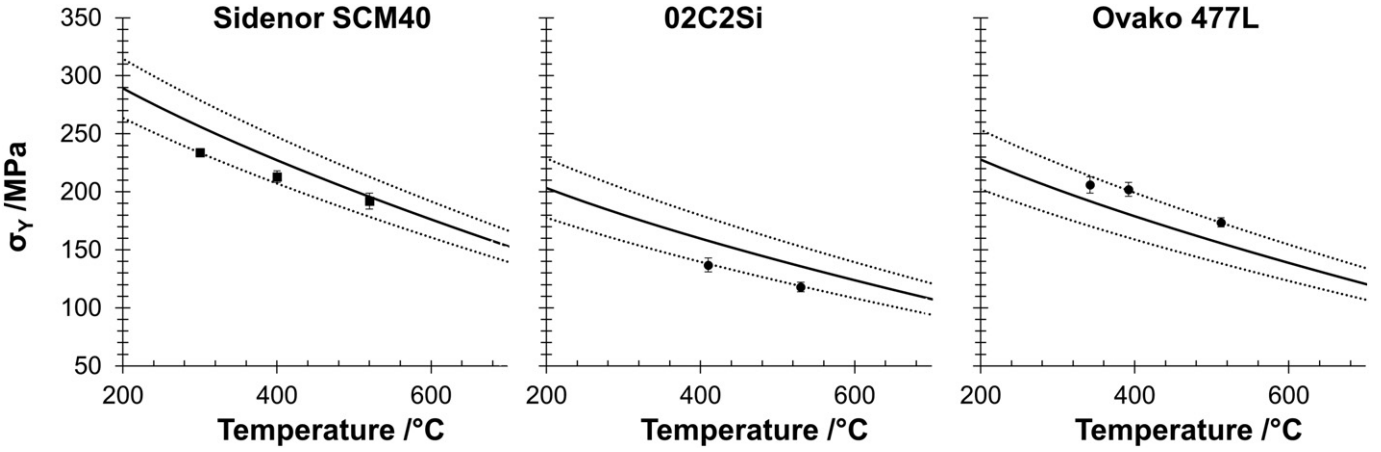

Fig. 8. Predicted vs. experimental yield strength as a function of temperature, where the continuous line represents the predicted yield strength by Eq. (18) and the dotted lines represent the variability of the prediction due to the variability of the Hall Petch strengthening assumed in this work. The experimental values and their 95% confidence errors are represented by dots and by their error bars.

5.3. Further validation with unseen experimental data

Single hit compression tests, already detailed in the Experimental section, allowed to further validate the model with experimental values of yield strengths of steels that were not included in the database. Several tests with different T_{def} were carried out for each of the steels. It was decided to maintain a fixed strain rate for all the steels, as the effect of the temperature is more evident that the effect of the strain rate, according to the study.

After obtaining the stress-strain curves, the yield strength was calculated by the 0.2% rule. Considering the steels chemical compositions and the imposed strain rate, the yield strength was calculated as a function of temperature by Eq. (18) as has been the one that has shown the lowest expected prediction error.

As can be seen in Fig. 8, predictions are accurate in most of the cases, as eight out of eight experimental yield strength values are in the area representing the yield strength prediction given by Eq. (18), validating the model.

6. Conclusion

1. The models proposed by Young et al. and van Bohemen are not able to predict yield strengths for temperatures above 960 and 1000 °C, respectively, and they do not take into account the effect of strain rate on the yield strength. Furthermore, they do not give accurate predictions of the austenite yield strengths for temperatures lower than their corresponding thresholds, even though their coefficients have physical meaning. In addition, their errors vary markedly depending on the tested ranges of composition and temperature. Whereas the modified Young et al.'s model seems to only be accurate for rather high carbon steels (1.36 and 2.21 at. % C) at low temperatures (family 3), the modified van Bohemen's model only gives accurate predictions for medium temperatures and not too high strain rates (families 2 and 3).
2. The proposed model, which has been proved to be physically consistent, gives much more accurate predictions of the σ_Y, it covers a much wider range of compositions and temperatures and, in addition, it includes the effect of the strain rate on the yield strength, parameter that had not yet been taken into account in similar models of the literature.
3. The expression in which the JC model has been included, Eq. (18), predicts the yield strength in a much more accurate way than the tested former models and the expression based on MZA, Eq. (19), even though the literature indicates that MZA is more accurate for any kind of strain rate or temperature. Also, the formulation in which the JC model was included, Eq. (16) was proved to be more generalizable than the one which was based on MZA, Eq. (17), by using the K-Fold Cross-Validation method. A good fitting has also been found for Eq. (18) when validating the model with data that were not included in the model.

Data availability

The raw/processed data required to reproduce these findings cannot be shared at this time due to technical or time limitations.

CRediT authorship contribution statement

Adriana Eres-Castellanos: Writing - original draft, Methodology, Software, Validation.**Isaac Toda-Caraballo:** Writing - review & editing, Conceptualization, Methodology, Supervision.**Andreas Latz:** Writing - review & editing, Resources.**Francisca G. Caballero:** Writing - review & editing, Supervision.**Carlos Garcia-Mateo:** Writing - review & editing, Supervision.

Declaration of competing interest

The authors declare that they have no known competing financial interests or personal relationships that could have appeared to influence the work reported in this paper.

Acknowledgements

The authors gratefully thank the contribution of: Thyssenkrupp Steel Europe AG, for providing 68% of the database, the Department of Mechanical Engineering of the École de technologie supérieure (ETS Montreal), the Group of Microstructures of the Delft University of Technology (TU Delft). This work was supported by the European Research Fund for Coal and Steel under the Contract RFCE-2015-709607 and by the Program Atracción de talento investigador (Consejería de Educación, Juventud y Deporte, Comunidad de Madrid), under the fellowship 2016-T2/IND-1693.

Appendix A

The K-Fold Cross-Validation estimator is a very common procedure in the field of applied machine learning to evaluate the performance of models which have been fitted with a limited dataset to generalize and accurately predict independent data. Usually, this procedure is used to compare two or more different models describing a given property. Once one model is selected, it can be calibrated by using the whole dataset.

As an exemplification, the procedure to compare two different models (f_1 and f_2) is subsequently described. It consists of the following steps which have also been schematized in Fig. A1.

1. Divide the whole data sets into K randomly generated folds or subsets.
2. Set the iteration number N as 1.
3. Set Fold N as testing fold, whereas the rest of the folds will be the training folds.
4. Train the models with the (1-K) training folds, obtaining the values of the parameters which describe both f_1 and f_2 for the current step, let us call them f_{1-N} and f_{2-N}.
5. Test the models with Fold 1, and calculate the MSE of both models for the current step, i.e. $MSE_{1\text{-}N}$ and $MSE_{2\text{-}N}$.
6. Increase N by 1 and repeat steps 3–5 until N=K.
7. When N=K, compute the expected prediction errors of f_1 and f_2, MSE_1 and MSE_2 respectively, by averaging all MSE computed during previous steps.
8. The best model in terms of generalization is the one which presents the lowest expected prediction error

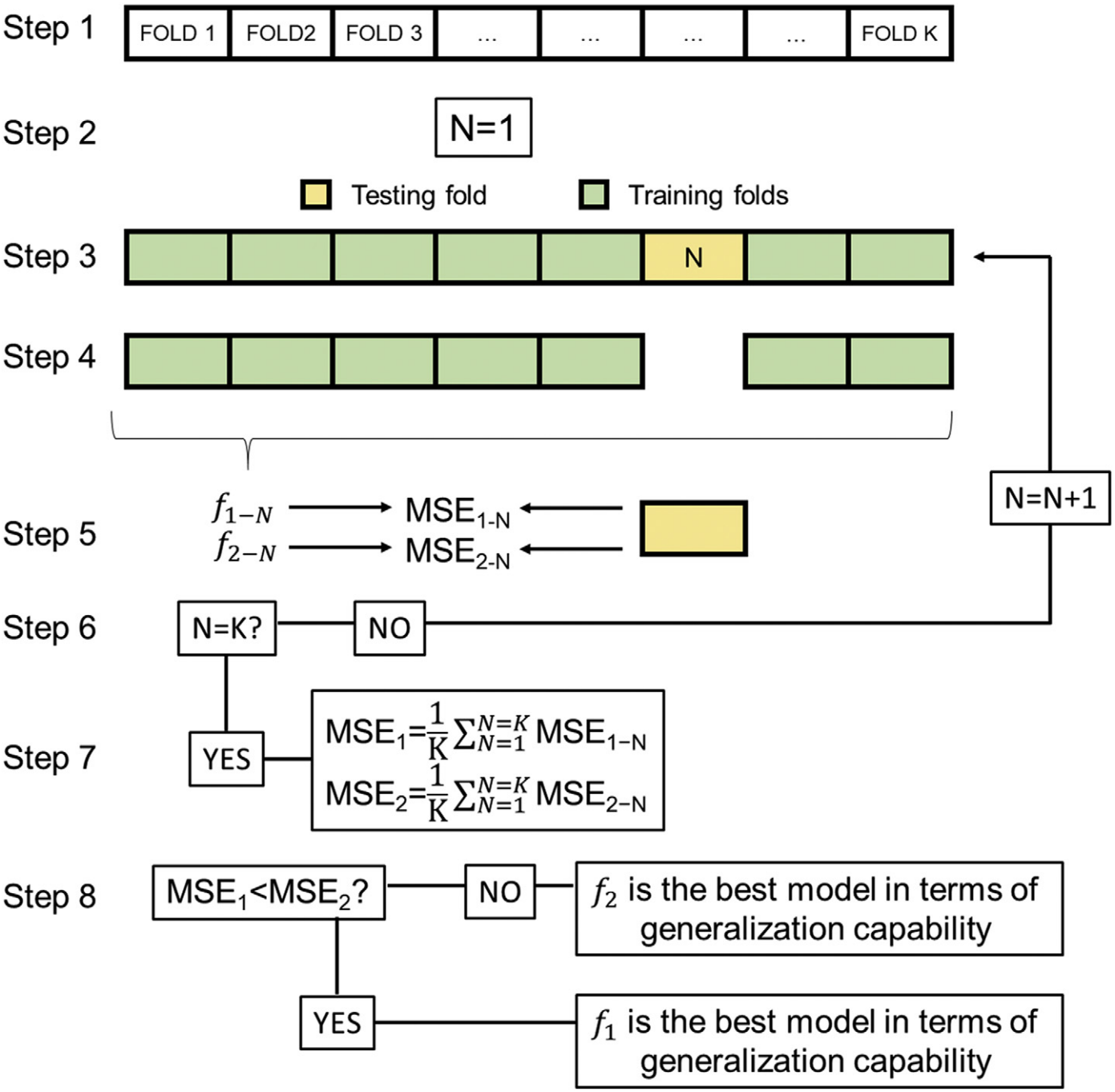

Fig. A1. Scheme showing the K-Fold Cross Validation procedure. Further information can be found in Appendix A.

References

[1] A. Arif, O. Khan, A. Sheikh, Roll deformation and stress distribution under thermo-mechanical loading in cold rolling, J. Mater. Process. Technol. 147 (2) (2004) 255–267.
[2] D. Jortner, J. Osterle, C. Zorowski, An analysis of cold strip rolling, Int. J. Mech. Sci. 2 (3) (1960) 179–194.
[3] S.B. Singh, H.K.D.H. Bhadeshia, Estimation of bainite plate-thickness in low-alloy steels, Mater. Sci. Eng. A 245 (1) (1998) 72–79.
[4] J. Cornide, C. Garcia-Mateo, C. Capdevila, F.G. Caballero, An assessment of the contributing factors to the nanoscale structural refinement of advanced bainitic steels, J. Alloys Compd. 577 (2013) S43–S47.
[5] W. Li, X. Zhang, H. Kou, R. Wang, D. Fang, Theoretical prediction of temperature dependent yield strength for metallic materials, Int. J. Mech. Sci. 105 (2016) 273–278.
[6] Y. Li, W. Li, X. Zhang, J. Ma, J. Shao, H. Kou, Y. Deng, Modeling of temperature dependent yield strength for stainless steel considering nonlinear behavior and the effect of phase transition, Constr. Build. Mater. 159 (2018) 147–154.
[7] S. Sevsek, W. Bleck, Ab initio-based modelling of the yield strength in high-manganese steels, Metals 8 (1) (2018) 34.
[8] H. Sieurin, J. Zander, R. Sandström, Modelling solid solution hardening in stainless steels, Mater. Sci. Eng. A 415 (1–2) (2006) 66–71.
[9] N.F. Fiore, C.L. Bauer, Binding of solute atoms to dislocations, Prog. Mater. Sci. 13 (1968) 85–134.
[10] M. Butt, P. Feltham, Solid-solution hardening, J. Mater. Sci. 28 (10) (1993) 2557–2576.
[11] P. Sivaprasad, S. Mandal, V. Sridhar, C. Narayanan, V. Shanmugam, B. Raj, Artificial neural network modelling of the tensile properties of indigenously developed 15 Cr-15 Ni-2. 2 Mo-Ti modified austenitic stainless steel, Trans. Indian Inst. Metals 59 (4) (2006) 437–445.
[12] R.K. Desu, H.N. Krishnamurthy, A. Balu, A.K. Gupta, S.K. Singh, Mechanical properties of austenitic stainless steel 304L and 316L at elevated temperatures, Journal of Materials Research and Technology 5 (1) (2016) 13–20.
[13] M.J. Peet, Neural network modelling of hot deformation of austenite, Materials Science and Metallurgy, University of Cambridge, 2001.
[14] K. Irvine, The strength of austenitic stainless steels, J. Iron Steel Inst. 207 (1969) 1017–1028.
[15] S. van Bohemen, Exploring the correlation between the austenite yield strength and the bainite lath thickness, Mater. Sci. Eng. A 731 (2018) 119–123.
[16] M. Azuma, N. Fujita, M. Takahashi, T. Senuma, D. Quidort, T. Lung, Modelling upper and lower bainite trasformation in steels, ISIJ Int. 45 (2) (2005) 221–228.
[17] C.H. Young, H.K.D.H. Bhadeshia, Strength of mixtures of bainite and martensite, Mater. Sci. Technol. 10 (3) (1994) 209–214.
[18] D. Walker, R. Honeycombe, Mechanical properties of metastable austenite in low-alloy steels, Met. Sci. 16 (8) (1982) 393–397.
[19] C. Garcia-Mateo, in: L. Duprez, G. Paul, M. Somani (Eds.),RFCS-2015-709607: "TIANOBAIN: Towards Industrial Applicability of (Medium C) Nanostructured Bainitic Steels", 2016-2020.
[20] t.S.E. AG, Internal database, 2019.
[21] D. Barraclough, C. Sellars, Static recrystallization and restoration after hot deformation of type 304 stainless steel, Met. Sci. 13 (3–4) (1979) 257–268.
[22] L. Mavropoulos, J. Jonas, Effect of the combined addition of Niobium and Boron on static recrystallization in hot worked austenite, Can. Metall. Q. 27 (3) (1988) 235–246.
[23] A. Laasraoui, J. Jonas, Recrystallization of austenite after deformation at high temperatures and strain rates—analysis and modeling, Metall. Trans. A. 22 (1) (1991) 151–160.
[24] R. Kaspar, J.S. Distl, O. Pawelski, Extreme austenite grain refinement due to dynamic recrystallization, Steel Res. Int. 59 (9) (1988) 421–425.
[25] G. Gottstein, M. Frommert, M. Goerdeler, N. Schäfer, Prediction of the critical conditions for dynamic recrystallization in the austenitic steel 800H, Mater. Sci. Eng. A 387 (2004) 604–608.
[26] R. Petković, M. Luton, J. Jonas, Recovery and recrystallization of carbon steel between intervals of hot working, Can. Metall. Q. 14 (2) (1975) 137–145.
[27] E. Hall, The deformation and ageing of mild steel: III discussion of results, Proc. Phys. Soc. London, Sect. B 64 (9) (1951) 747.
[28] E. Hall, Yield Point Phenomena in Metals and Alloys, Springer Science & Business Media, 2012.
[29] H.K.D.H. Bhadeshia, R.W.K. Honeycombe, Steels: Microstructure and Properties, Butterworths-Heinemann (Elsevier), 2006.
[30] P. Kusakin, A. Belyakov, D.A. Molodov, R. Kaibyshev, On the effect of chemical composition on yield strength of TWIP steels, Mater. Sci. Eng. A 687 (2017) 82–84.
[31] O. Bouaziz, H. Zurob, B. Chehab, J. Embury, S. Allain, M. Huang, Effect of chemical composition on work hardening of Fe—Mn—C TWIP steels, Mater. Sci. Technol. 27 (3) (2011) 707–709.
[32] M.N. Yoozbashi, S. Yazdani, T.S. Wang, Design of a new nanostructured, high-Si bainitic steel with lower cost production, Mater. Des. 32 (6) (2011) 3248–3253.
[33] P.E.J. Rivera-Díaz-Del-Castillo, K. Hayashi, E.I. Galindo-Nava, Computational design of nanostructured steels employing irreversible thermodynamics, Mater. Sci. Technol. 29 (10) (2013) 1206–1211.
[34] M. Shah, S.K. Das, An artificial neural network model to predict the bainite plate thickness of nanostructured bainitic steels using an efficient network-learning algorithm, J. Mater. Eng. Perform. 27 (11) (2018) 5845–5855.
[35] L.M. Rivas, Microstructure and Mechanical Response of Nanostructured Bainitic Steels, CSIC - Centro Nacional de Investigaciones Metalúrgicas (CENIM) Universidad Carlos III de Madrid, 2016.
[36] H.K.D.H. Bhadeshia, Bainite in Steels: Theory and Practice, 3 ed. Maney Publishing, 2015.
[37] J.C. Lagarias, J.A. Reeds, M.H. Wright, P.E. Wright, Convergence properties of the Nelder–Mead simplex method in low dimensions, SIAM J. Optim. 9 (1) (1998) 112–147.
[38] G.R. Johnson, A constitutive model and data for materials subjected to large strains, high strain rates, and high temperatures, Proc. 7th Inf. Sympo. Ballistics 1983, pp. 541–547.
[39] G.R. Johnson, W.H. Cook, Fracture characteristics of three metals subjected to various strains, strain rates, temperatures and pressures, Eng. Fract. Mech. 21 (1) (1985) 31–48.
[40] F.J. Zerilli, R.W. Armstrong, Dislocation-mechanics-based constitutive relations for material dynamics calculations, J. Appl. Phys. 61 (5) (1987) 1816–1825.
[41] R. Liang, A.S. Khan, A critical review of experimental results and constitutive models for BCC and FCC metals over a wide range of strain rates and temperatures, Int. J. Plast. 15 (9) (1999) 963–980.
[42] A.S. Khan, Y.S. Suh, R. Kazmi, Quasi-static and dynamic loading responses and constitutive modeling of titanium alloys, Int. J. Plast. 20 (12) (2004) 2233–2248.
[43] S. Nemat-Nasser, W.-G. Guo, Thermomechanical response of DH-36 structural steel over a wide range of strain rates and temperatures, Mech. Mater. 35 (11) (2003) 1023–1047.
[44] N. Kotkunde, A.D. Deole, A.K. Gupta, S.K. Singh, Comparative study of constitutive modeling for Ti–6Al–4V alloy at low strain rates and elevated temperatures, Mater. Des. 55 (2014) 999–1005.
[45] D. Samantaray, S. Mandal, U. Borah, A. Bhaduri, P. Sivaprasad, A thermo-viscoplastic constitutive model to predict elevated-temperature flow behaviour in a titanium-modified austenitic stainless steel, Mater. Sci. Eng. A 526 (1–2) (2009) 1–6.
[46] H. Zhan, G. Wang, D. Kent, M. Dargusch, Constitutive modelling of the flow behaviour of a β titanium alloy at high strain rates and elevated temperatures using the Johnson–Cook and modified Zerilli–Armstrong models, Mater. Sci. Eng. A 612 (2014) 71–79.
[47] W.K. Rule, S. Jones, A revised form for the Johnson–Cook strength model, Int. J. Impact Eng. 21 (8) (1998) 609–624.
[48] D. Samantaray, S. Mandal, A. Bhaduri, A comparative study on Johnson Cook, modified Zerilli–Armstrong and Arrhenius-type constitutive models to predict elevated temperature flow behaviour in modified 9Cr–1Mo steel, Comput. Mater. Sci. 47 (2) (2009) 568–576.
[49] Y. Lin, X.-M. Chen, A critical review of experimental results and constitutive descriptions for metals and alloys in hot working, Mater. Des. 32 (4) (2011) 1733–1759.
[50] Y. Wang, C.-j. Han, C. Wang, S.-k. Li, A modified Johnson–Cook model for 30Cr2Ni4MoV rotor steel over a wide range of temperature and strain rate, J. Mater. Sci. 46 (9) (2011) 2922–2927.
[51] Y. Lin, X.-M. Chen, G. Liu, A modified Johnson–Cook model for tensile behaviors of typical high-strength alloy steel, Mater. Sci. Eng. A 527 (26) (2010) 6980–6986.
[52] Y. Lin, Q.-F. Li, Y.-C. Xia, L.-T. Li, A phenomenological constitutive model for high temperature flow stress prediction of Al–Cu–Mg alloy, Mater. Sci. Eng. A 534 (2012) 654–662.
[53] J. Cai, K. Wang, P. Zhai, F. Li, J. Yang, A modified Johnson-Cook constitutive equation to predict hot deformation behavior of Ti-6Al-4V alloy, J. Mater. Eng. Perform. 24 (1) (2015) 32–44.
[54] M. Vural, J. Caro, Experimental analysis and constitutive modeling for the newly developed 2139-T8 alloy, Mater. Sci. Eng. A 520 (1–2) (2009) 56–65.
[55] H. Zhang, W. Wen, H. Cui, Y. Xu, A modified Zerilli–Armstrong model for alloy IC10 over a wide range of temperatures and strain rates, Mater. Sci. Eng. A 527 (1–2) (2009) 328–333.
[56] F.H. Abed, G.Z. Voyiadjis, A consistent modified Zerilli-Armstrong flow stress model for BCC and FCC metals for elevated temperatures, Acta Mech. 175 (1–4) (2005) 1–18.
[57] Y. Lin, X.-M. Chen, A combined Johnson–Cook and Zerilli–Armstrong model for hot compressed typical high-strength alloy steel, Comput. Mater. Sci. 49 (3) (2010) 628–633.
[58] T. Byun, N. Hashimoto, K. Farrell, Temperature dependence of strain hardening and plastic instability behaviors in austenitic stainless steels, Acta Mater. 52 (13) (2004) 3889–3899.
[59] V. Gavriljuk, A. Sozinov, J. Foct, J.N. Petrov, Y.A. Polushkin, Effect of nitrogen on the temperature dependence of the yield strength of austenitic steels, Acta Mater. 46 (4) (1998) 1157–1163.
[60] Y.-S. Kim, S. Nam, S.-J. Kim, Strain rate dependence of deformation behavior of high-nitrogen austenitic steels, J. Mater. Process. Technol. 187 (2007) 575–577.
[61] D. Samantaray, S. Mandal, A. Bhaduri, S. Venugopal, P. Sivaprasad, Analysis and mathematical modelling of elevated temperature flow behaviour of austenitic stainless steels, Mater. Sci. Eng. A 528 (4–5) (2011) 1937–1943.
[62] D. Samantaray, S. Mandal, C. Phaniraj, A. Bhaduri, Flow behavior and microstructural evolution during hot deformation of AISI Type 316 L (N) austenitic stainless steel, Mater. Sci. Eng. A 528 (29–30) (2011) 8565–8572.
[63] H.-Y. Li, X.-F. Wang, D.-D. Wei, J.-D. Hu, Y.-H. Li, A comparative study on modified Zerilli–Armstrong, Arrhenius-type and artificial neural network models to predict high-temperature deformation behavior in T24 steel, Mater. Sci. Eng. A 536 (2012) 216–222.
[64] H.-Y. Li, Y.-H. Li, X.-F. Wang, J.-J. Liu, Y. Wu, A comparative study on modified Johnson Cook, modified Zerilli–Armstrong and Arrhenius-type constitutive models to predict the hot deformation behavior in 28CrMnMoV steel, Mater. Des. 49 (2013) 493–501.
[65] D. Samantaray, A. Patel, U. Borah, S. Albert, A. Bhaduri, Constitutive flow behavior of IFAC-1 austenitic stainless steel depicting strain saturation over a wide range of strain rates and temperatures, Materials & Design (1980–2015) 56 (2014) 565–571.
[66] L. Schwer, Optional Strain-rate Forms for the Johnson Cook Constitutive Model and the Role of the Parameter Epsilon_0, 6th European LS-DYNA Users' Conference, Frankenthal, Germany, Oct, 2007 11–22.
[67] Y. Matsuoka, T. Iwasaki, N. Nakada, T. Tsuchiyama, S. Takaki, Effect of grain size on thermal and mechanical stability of austenite in metastable austenitic stainless steel, ISIJ Int. 53 (7) (2013) 1224–1230.

[68] C. Celada-Casero, J. Sietsma, M.J. Santofimia, The role of the austenite grain size in the martensitic transformation in low carbon steels, Mater. Des. 167 (2019), 107625.
[69] D. Xu, C. Ji, H. Zhao, D. Ju, M. Zhu, A new study on the growth behavior of austenite grains during heating processes, Sci. Rep. 7 (1) (2017) 3968.
[70] S. Rajasekhara, P. Ferreira, L. Karjalainen, A. Kyröläinen, Hall–Petch behavior in ultra-fine-grained AISI 301LN stainless steel, Metall. Mater. Trans. A 38 (6) (2007) 1202–1210.
[71] R. Naybour, Hardening during deformation of an 18Cr/12Ni/Nb austenitic steel at 650°C, Acta Metall. 13 (11) (1965) 1197–1207.
[72] S.N. Monteiro, F.M. Margem, V.S. Candido, A.B.-H. Figueiredo, High temperature plastic instability and dynamic strain aging in the tensile behavior of AISI 316 stainless steel, Mater. Res. 20 (2017) 506–511.
[73] J. Bressanelli, A. Moskowitz, Effects of strain rate, temperature, and composition on tensile properties of metastable austenitic stainless steels, ASM Trans Quart 59 (2) (1966) 223–239.
[74] M. Stone, Cross-validatory choice and assessment of statistical predictions, J. R. Stat. Soc. Ser. B Methodol. 36 (2) (1974) 111–133.
[75] R. Kohavi, A Study of Cross-validation and Bootstrap for Accuracy Estimation and Model Selection, Ijcai, Montreal, Canada, 1995 1137–1145.
[76] J.-H. Kang, T. Ingendahl, J. von Appen, R. Dronskowski, W. Bleck, Impact of short-range ordering on yield strength of high manganese austenitic steels, Mater. Sci. Eng. A 614 (2014) 122–128.
[77] R. Labusch, A statistical theory of solid solution hardening, Phys. Status Solidi B 41 (2) (1970) 659–669.
[78] I. Toda-Caraballo, A general formulation for solid solution hardening effect in multi-component alloys, Scr. Mater. 127 (2017) 113–117.
[79] I. Toda-Caraballo, P.E. Rivera-Díaz-del-Castillo, Modelling solid solution hardening in high entropy alloys, Acta Mater. 85 (2015) 14–23.
[80] M.P. Agustianingrum, I. Ondicho, D.E. Jodi, N. Park, U. Lee, Theoretical evaluation of solid solution interaction in Fex (CoCrMnNi) 100-x medium-and high-entropy alloys, Mater. Sci. Eng. A 759 (2019) 633–639.
[81] W.B. Pearson, A Handbook of Lattice Spacings and Structures of Metals and Alloys: International Series of Monographs on Metal Physics and Physical Metallurgy, Elsevier, 2013.